Strojniški vestnik - Journal of Mechanical Engineering 68(2022)7-8, 493-505
DOI:10.5545/sv-jme.2022.142
Original Scientific Paper
Received for review: 2022-03-31
Received revised form: 2022-05-30
Accepted for publication: 2022-06-01

Effect of Dual-stage Ageing and RRA Treatment on the Three-body Abrasive Wear of the AW7075 Alloy

Marzena M. Lachowicz* − Tadeusz Leśniewski − Maciej B. Lachowicz
Wroclaw University of Science and Technology, Faculty of Mechanical Engineering, Poland

The paper presents an analysis of the influence of the heat treatment state on the abrasive wear of the AW7075 aluminium alloy. To determine the hardening state, the material hardness was measured. It was found that hardness is not the only factor that influences this type of wear. For this reason, the influence of the emerging microstructure is also analysed in the considerations. After tribological tests, microscopic observations of surface features were carried out to determine the dominant mechanisms of surface damage. The results were extended by the hardness distribution carried out on the cross-section. There were no changes in hardness that could be related to either strain hardening or structural changes caused by friction.

Keywords: aluminium alloys, AW7075, abrasive wear, heat treatment, hardness, microstructure

Highlights

- *The hardness of the AW7075 alloy is not the only determinant of abrasive wear; with the microstructure of the tested alloy and the related heat treatment, the state also plays an important role in this respect.*
- *The abrasive wear of the tested alloy can be ranked in the following order according to the heat treatment condition: dual ageing < RRA treatment < T6 state.*
- *The wear features show a similar type of damage, regardless of the heat treatment state. Scratches, grooves, microcracks, and slight plastic deformation features be observed on the wear surface.*
- *Decohesion developed mainly around grain boundaries and interfacial boundaries, which facilitates the loss of continuity with the matrix in the presence of coherent particles. Larger and incoherent precipitates in the matrix can act as an abrasive and increase the wear rate.*
- *The presence of large particles of the primary phases, which do not dissolve at the stage of heat treatment, promotes their crushing and defragmentation during abrasive wear.*
- *The surface hardness does not change due to the occurrence of mechanical effects resulting from friction.*

0 INTRODUCTION

There is relative movement between surfaces of components in some applications of aluminium alloys. Wear resistance then becomes an important property to consider. Numerous research studies show that heat treatment can have a significant impact on tribological wear. In particular, the fragmentation of the microstructure components can significantly affect the obtained tribological parameters **[1]** to **[3]**.

The presence of intermetallic phases in the microstructure offers a wide spectrum of possibilities for the strengthening of aluminium alloys. This group also includes the high-strength 7000 series alloys. Two treatments are used for this purpose: supersaturation and subsequent ageing. The sequence for ageing the 7000 series alloys is given as follows: solid solution (α) → Guinier-Preston (GP) zones → η' ($MgZn_2$) → η ($MgZn_2$) **[4]** and **[5]**. The typical hardness-ageing diagram for a heat-treatable aluminium alloy is shown in Fig. 1. GP zones are formed during ageing at room temperature or the early stages of ageing. They are fully coherent with the matrix. The greatest hardening effect is achieved at the stage of separation of the intermediate phase, which is related to the change in the mechanism of the interaction of the precipitates with dislocations. This is a typical T6 state. The stresses that are needed to cut the particles by dislocation, as well as the stresses caused by the Orowan mechanism associated with the formation of a dislocation loop around these precipitates, obtain their maximum values. The material hardness drops significantly when there is a complete loss of the coherence of the precipitates. Ageing to the T6 state is associated with a continuous distribution of grain boundary precipitates (GBPs) **[6]** and **[7]**. A properly carried out heat treatment should end at the stage of forming the matrix of precipitates (MPs), which is partially coherent with the intermediate phase η'.

The T6 state is characterized by high strength and hardness but is highly susceptible to stress corrosion cracking. When looking for greater resistance to this type of corrosion, dual-stage ageing (DA) and Retrogression and Re-Ageing (RRA) treatment are used **[9]** to **[13]**. The first stage of DA ageing is characterized by a lower temperature when compared

*Corr. Author's Address: Wroclaw University of Science and Technology, Faculty of Mechanical Engineering, Department of Metal Forming, Welding Technology and Metrology, Lukasiewicza 7-9, 50-371 Wroclaw, Poland, marzena.lachowicz@pwr.edu.pl

to conventional ageing, and it is responsible for the diffusion and homogeneous distribution of the GP zones. The coarse-grained GP zones and phases are formed during the second ageing and contribute to the peak hardness. MPs are coarser and partially incoherent with phase η when compared to one-step ageing. This helps to reduce the hardness of the alloy [12] and [13]. Another solution is the multi-stage RRA heat treatment. Retrogression involves heating the alloy, which had earlier been hardened, at a temperature in the range of 200 ºC to 260 ºC for a short period (120 s), and then re-ageing the alloy to a condition typical for the T6 state. The use of the RRA treatment leads to the obtaining of a microstructure that is characterized by the presence of fine-dispersed and coherent η' ($MgZn_2$) MPs. They are characteristic of the T6 state. However, at the GBPs there are fragmented and discontinuous precipitations that are typical for T7 over-ageing. As a result, the grain boundary that is line blocked with continuous GBPs particles, as in the T6 state, is transformed into a state in which the precipitates of the η phase are coarse and discontinuous [9], [14], and [15]. After the RRA treatment, a larger fraction of the GBPs was observed [7]. Also, the copper content of GBPs increases with the time of heat treatment [6].

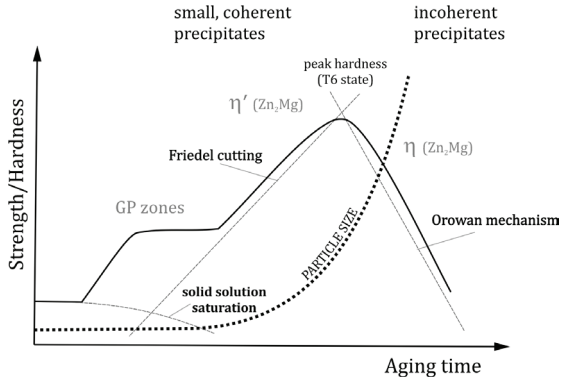

Fig. 1. *Schematic illustration of the precipitate strengthening contributions as a function aging time (based on [8])*

The effect of heat treatment of aluminium alloys on their strength is already known. Its influence on the resistance to structural corrosion is also well understood [12] to [16]. Retrogression and re-ageing treatment improve the resistance to stress corrosion cracking (SCC) [6], while maintaining high strength, until the MPs become coarse [6]. However, the microstructure changes caused by heat treatment affect other functional properties of aluminium alloys. The high strength is maintained as long as the MPs are not coarse [6]. The RRA state is characterized by high resistance to fatigue crack initiation and better impact toughness as a result of the increased discretion of the precipitates occurring at the grain boundaries [9], [17] and [18]. Coarse GBPs also increase electrical conductivity [9]. The DA state, in terms of microstructure, brings the alloy closer to the over-ageing condition, which in turn results in a reduction in strength and an increase in ductility [19]. It seems obvious that the different hardnesses obtained for individual states should also affect the tribological wear. For this reason, in the present study, it was decided to consider the influence of microstructure on the abrasive wear of the AW 7075 aluminium alloy.

1 MATERIAL AND METHODS

The tests were carried out on the AW 7075 aluminium alloy. The chemical composition of the alloy, which was determined by GDS-500A Leco glow discharge optical spectrometry (GD OES), is shown in Table 1.

In the microstructure of all the tested samples, α(Al) solid solution was observed with grey, large precipitates of the α-AlFeMnSi phase, and dark primary precipitates of the Mg_2Si phase (Fig. 2). The type of these particles was determined on the basis of the EDS results conducted as part of the preliminary studies and compared with the literature data. The grains of the solid solution were heterogeneous in nature and were surrounded by large precipitates of the iron-rich phase. The main changes in the microstructure, which were caused by the applied heat treatment, concern the morphology, size, quantity, and coherence of the formed precipitates. For this reason, the microstructure of the material in the image of the light microscope was of a similar nature. These changes are subtle and can, therefore, only be observed with the use of transmission electron microscopy (TEM) methods. However, it can be seen that in the case of the DA state, the precipitations of the strengthening phases are more clearly visible, which indicates their larger dimensions.

Table 1. *Chemical composition of the tested AW7075 aluminium alloy*

Element	Zn	Mg	Cu	Fe	Cr	Si	Mn	Ti	Al
Content [%]	5.42	2.34	1.45	0.39	0.26	0.12	0.10	0.03	rest

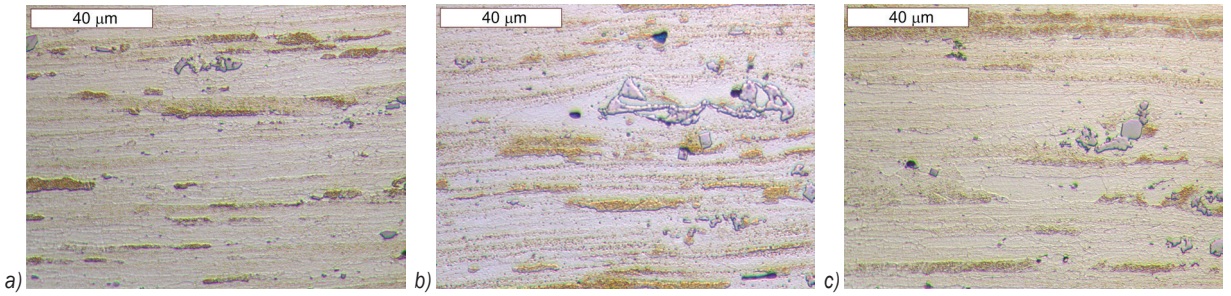

Fig. 2. *Microstructure after; a) T6, b) DA, and c) RRA, light microscopy, etched with 10 % HF*

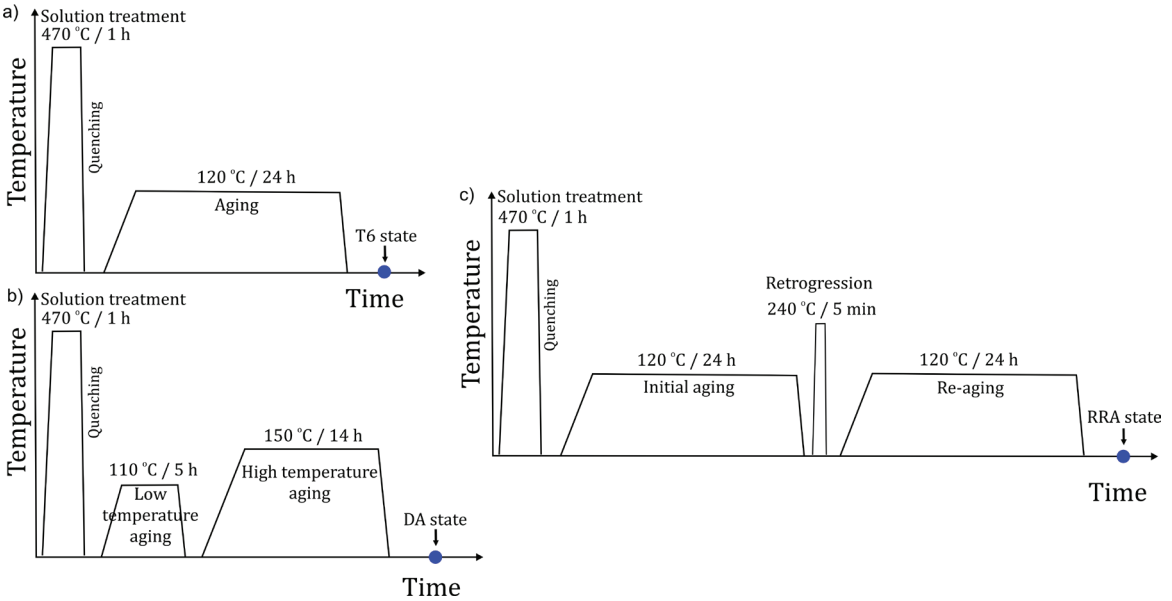

Fig. 3. *Flow chart for the heat treatment process; a) T6, b) DA, and c) RRA*

The parameters of three various heat treatments were developed for 30 mm × 100 mm sections with a thickness of 10 mm that were cut from the tested alloy (Fig. 3). The microstructure was investigated on conventionally prepared metallographic microsections using a Leica DM6000M light microscope. The tests were carried out before and after etching with a 10 % aqueous solution of HF. To determine the material hardening, BHN hardness measurements were carried out using the Brinell method and a DuraJet G5 hardness tester (Struers).

To determine the abrasive wear resistance, tests were carried out on the T-07 tester made at the Institute of Sustainable Technology in Radom (Poland). The tribological tests were performed in the presence of the loose F90 electro-corundum abrasive, and all the tested samples were subjected to the same friction conditions. The used abrasive reflects the penetration of aluminium oxide or anodic coatings into the friction area very well. The oxide film is thin and can break off easily, in turn producing wear debris particles. The removal of the protective layer also accelerates the corrosive effects [20]. The method complied with the requirements of the GOST 23.208-79 standard [21].

The tested system consisted of a sample (plate) made of the tested material, and a counter-sample (roll) with a rubber ring. During the test, the material sample was pressed with a defined force of (F_N) to a rubber disk with a diameter of d = 50 mm, which was rotating at a constant speed (n). Gravity was used to deliver a loose abrasive between the rotating disc and the fixed sample. In the presence of loose abrasive, the sample of the tested materials and the reference sample were subjected to abrasive wear under the used operating conditions, i.e., rotational speed n = 60 rpm/min, test time t, and F_N loads in accordance with the above standard (t = 10 min, F = 44 N). The reference sample was grade C45 normalized steel. Next, the mass loss of the reference sample (Z_{ww}) and the mass loss of the tested materials (Z_{wb}) were

determined. The mass loss of the samples (weight difference before and after the tests) was determined after a defined test time (determined by the number of rotations of the rubber roller). Based on the mass loss measurements, the abrasive wear resistance index K_b (relative wear resistance) was calculated from the following equation (Eq. (1)):

$$K_b = \frac{Z_{ww} \cdot \rho_b \cdot N_b}{Z_{wb} \cdot \rho_w \cdot N_w}, \quad (1)$$

where Z_{ww} is the mass loss of the reference material (C45 steel), Z_{wb} the mass loss of the tested material, ρ_w the density of the reference material, ρ_b the density of the tested material, N_w the number of revolutions of the reference material's friction path, and N_b the number of revolutions of the tested material's friction path. The density of the tested material (AW 7075) was 2.81 g/cm³.

The morphology of the specimens after the tribological tests was observed using scanning electron microscopy (SEM), which also identified the wear features. The Phenom World ProX microscope was used for this purpose. Backscattered electrons (BSE) and second electrons (SE) detectors with an accelerating voltage of 15 kV were used.

2 RESULTS AND DISCUSSION

2.1 Hardness Measurements

Based on the performed measurements, it can be stated that the proposed heat treatment contributed to the material strengthening (Fig. 4). It was found that the Brinell hardness (BHN) of the AW7075 alloy increases in the following order: DA<T6<RRA. The highest hardness of the AW7075 alloy was obtained after the RRA heat treatment, while the alloy that was heat treated to the T6 state had a slightly lower hardness. The use of double-stage ageing adversely affected the alloy strengthening, with the hardness after this process being the lowest.

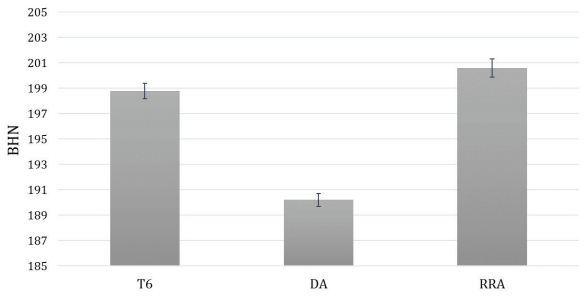

Fig. 4. *Results of hardness measurements of the AW 7075 alloy after various heat treatments*

2.2 Abrasive Wear

The AW 7075 aluminium alloy, with different levels of hardness obtained by heat treatment, was tested. Figs. 5 and 6 present the three-body dry abrasion of the AW 7075 alloy, which was determined as the weight loss for its heat-treated state. The results of the hardness and abrasive wear measurements can be summarized as follows:

- the abrasive wear kinetics of the T6 state were lower than for the DA and RRA states,
- the DA and RRA states, despite having different hardness values, had a comparable wear resistance,
- the hardest sample (RRA state) had worse wear resistance than the one with lower hardness (T6 state).

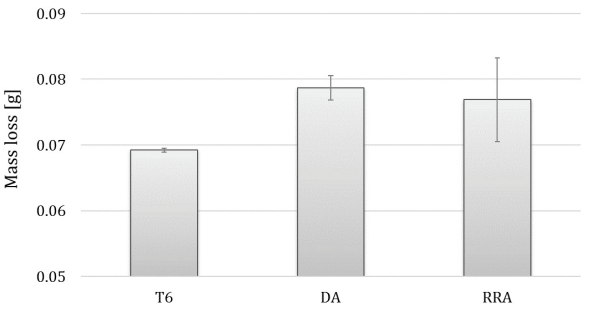

Fig. 5. *Mass loss (Z_{wb}) results obtained for the AW 7075 alloy after various heat treatments*

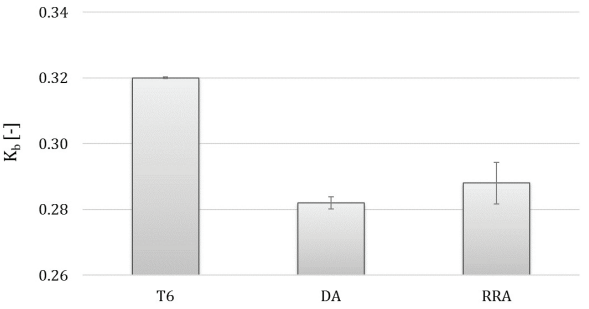

Fig. 6. *K_b factor obtained for the AW 7075 alloy after various heat treatments*

Linear wear low theory (also called Archard's equation) indicates the relationship between the hardness of the material and its abrasive wear resistance. In the case of the alloys in the DA state with the lowest hardness, the greatest weight loss, and thus the lowest wear resistance, was observed. However, in the remaining cases, this relationship did not work. Other authors also note that the correlation between hardness and wear resistance is not always

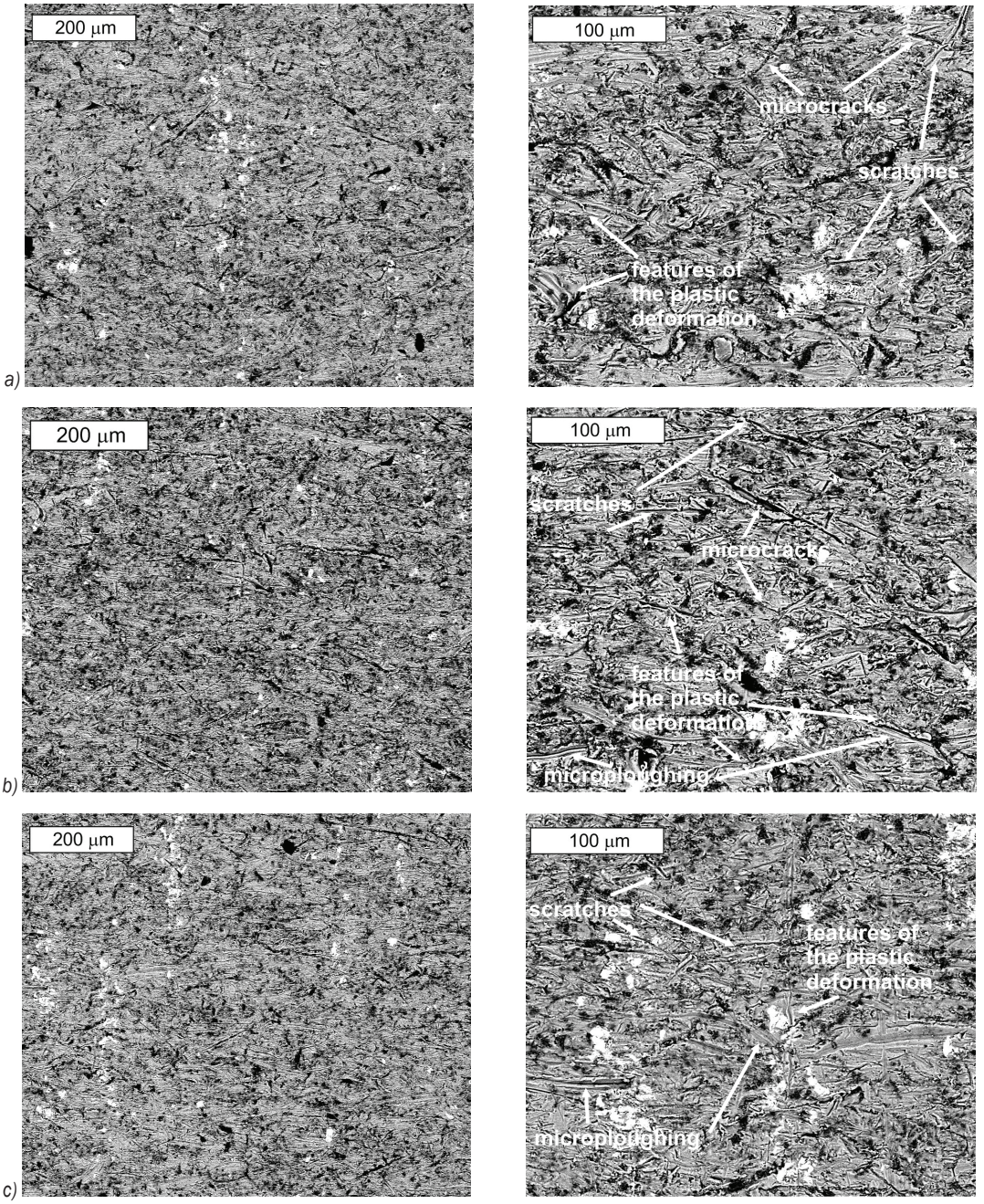

Fig. 7. *General views of the wear features after the different heat treatments; a) T6, b) DA, and c) RRA, SEM*

clear [22] to [24]. However, Archard did not consider the role of the microstructure as one of the key factors in abrasive wear.

The conducted research shows that the hardness of the AW 7075 alloy is not the only factor that determines its wear. No linear relationship was observed between the hardness of the material and its wear; therefore, it can be concluded that the wear is also determined by the microstructure of the material. From the point of view of the microstructure, aluminium alloys can be considered as "composites" that consist of a soft matrix and hard precipitates formed during the heat treatment stage, which in turn affect the hardness and strength of these alloys. The presence of hard particles in the matrix effectively reduces wear [25] and [26]. Microstructural parameters (e.g., the hardness, shape, size, volume fraction, and distribution of the second phases), the properties of

the matrix, and the interfacial bonding between the second phase and the matrix significantly influence the abrasive wear resistance [27]. Even a subtle change in the size and distribution of these precipitates can significantly affect the AW7075 alloy's operational properties.

It is not difficult to observe that the wear was lower in the states in which the microstructure mainly shows significant precipitation that is coherent with the matrix (T6 state). Literature data clearly indicate that in the T6 condition, GBPs are mainly continuous and coherent particles [6] and [7]. The hardening peak caused by the presence of coherent phases is also confirmed by hardness measurements (Fig. 4). During micro-ploughing, the metallic material is mainly elastically-plastically deformed, and it flows around and beneath the sliding particle [27]. In an ideal case, micro-ploughing, due to a single pass of one abrasive particle, does not result in any detachment of material from the wearing surface. A prow is formed ahead of the abrading particle, and the material is continuously displaced sideways to form ridges adjacent to the produced groove. As shown in Fig. 1, the particles coherent with the matrix will be sheared in accordance with the Friedel effect. This is conducive to maintaining the continuity of the matrix as well as the precipitations. Consequently, these particles are more difficult to detach from the matrix. In this situation, the wear will be mainly caused by foreign abrasive particles that are involved in the abrasion, which contributes to reduced consumption and higher K_b ratios. For both the RRA treatment and the T6 state, the particles that are partially coherent with the matrix constitute a significant contribution to the microstructure. The high degree of strengthening after RRA treatment is confirmed by high hardness (Fig. 4). However, after RRA treatment, the MPs are similar to those occurring in the T6 state [6], [7], [9], [14], and [15]. The grain boundaries are close to the over-ageing state. The GBPs consist of incoherent, discontinuous, and coarse precipitations [6], [7], [9], [14], [15], and [19]. In a situation in which a significant amount of precipitation is incoherent with the matrix, their presence in the microstructure may contribute to the decohesion of the material. However, it has been proved that a too high concentration of MPs deteriorates the resistance to stress corrosion cracking [6]. Material may be ploughed aside repeatedly by displacing particles, which may then detach due to micro-fatigue. The precipitations torn out in this

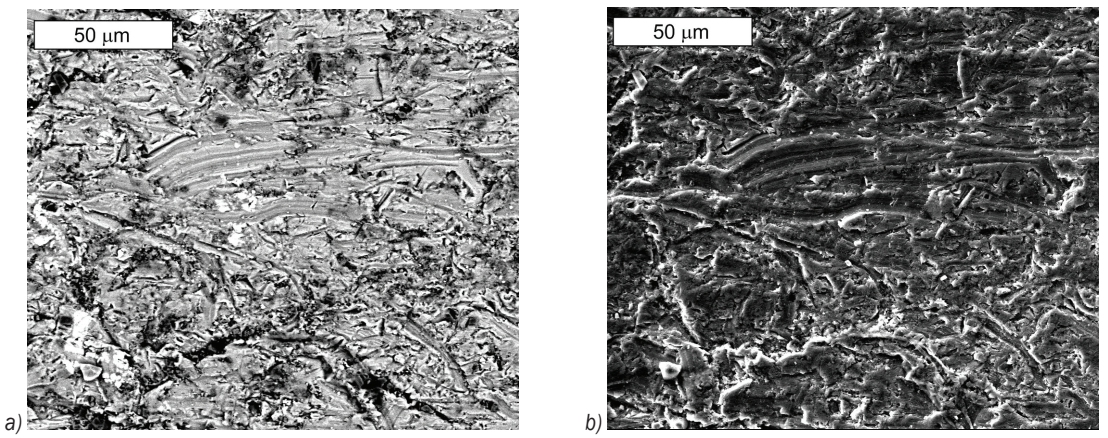

Fig. 8. *Wear morphology after the T6 heat treatment; SEM; a) BSE, and b) SE*

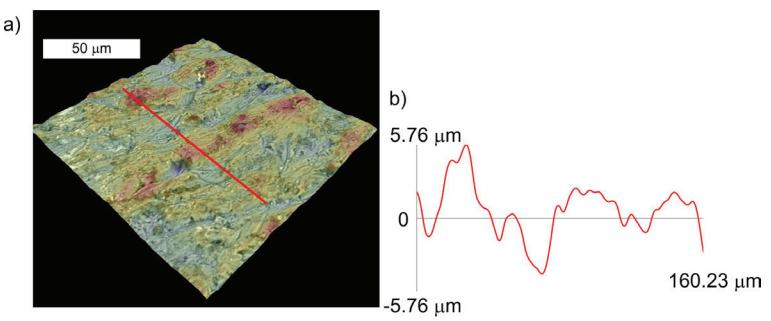

Fig. 9. *a) Exemplary SEM 3D-profilometry image, and b) surface texture of the wear tracks after the T6 heat treatment*

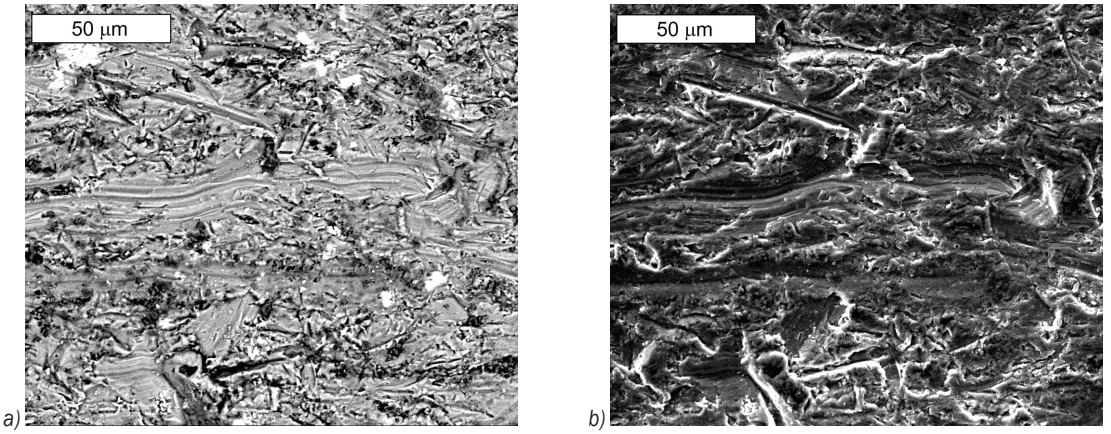

Fig. 10. *Wear morphology after DA, SEM a) BSE, and b) SE*

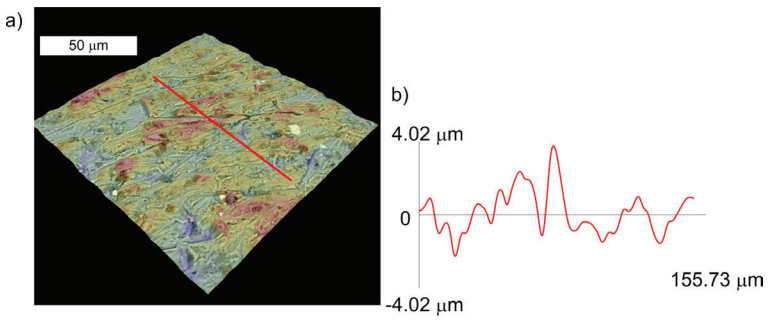

Fig. 11. *a) Exemplary SEM 3D-profilometry image, and b) the surface texture of the wear tracks after the DA heat treatment*

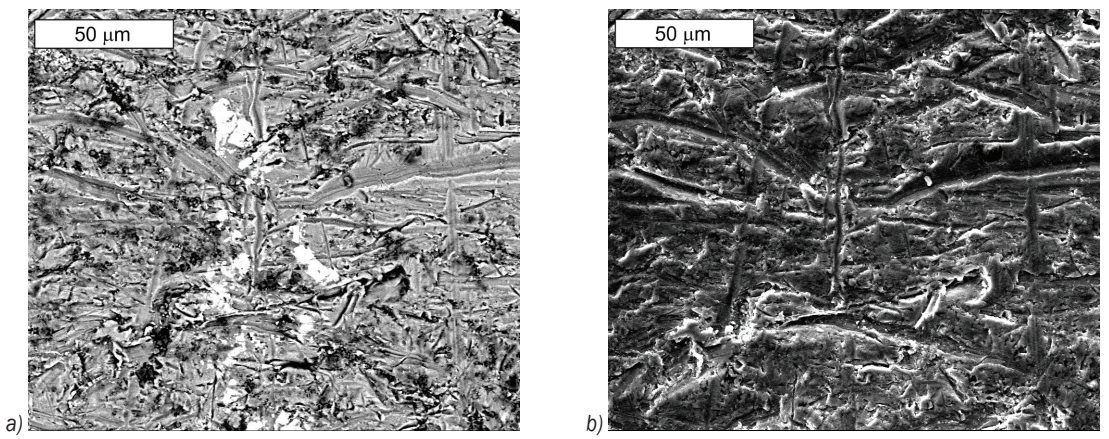

Fig. 12. *Wear morphology after RRA, SEM a) BSE, and b) SE*

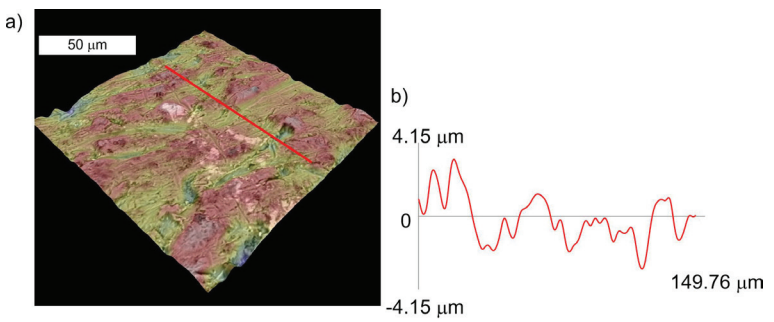

Fig. 13. *a) Exemplary SEM 3D-profilometry image, and b) the surface texture of the wear tracks after the RRA heat treatment*

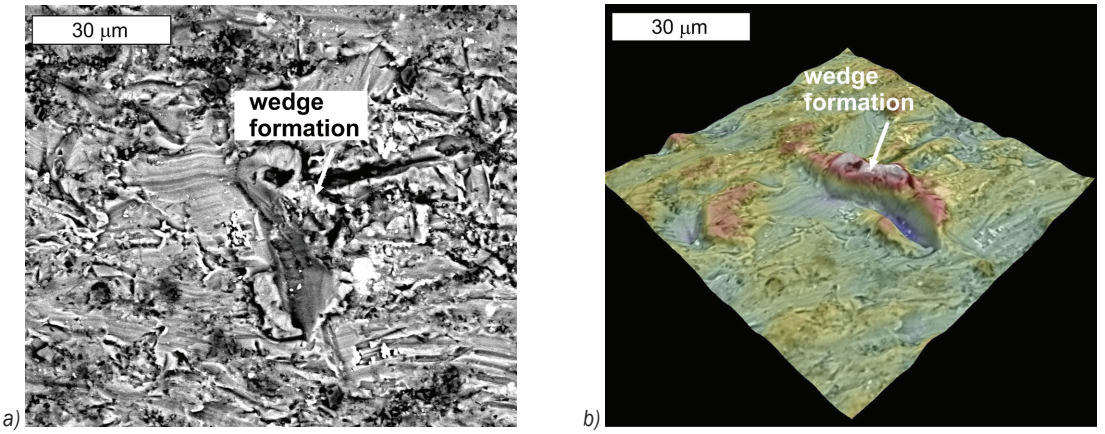

Fig. 14. *Wear morphology after DA; the wedge formation is visible locally; a) SEM image, and b) SEM 3D-profilometry image*

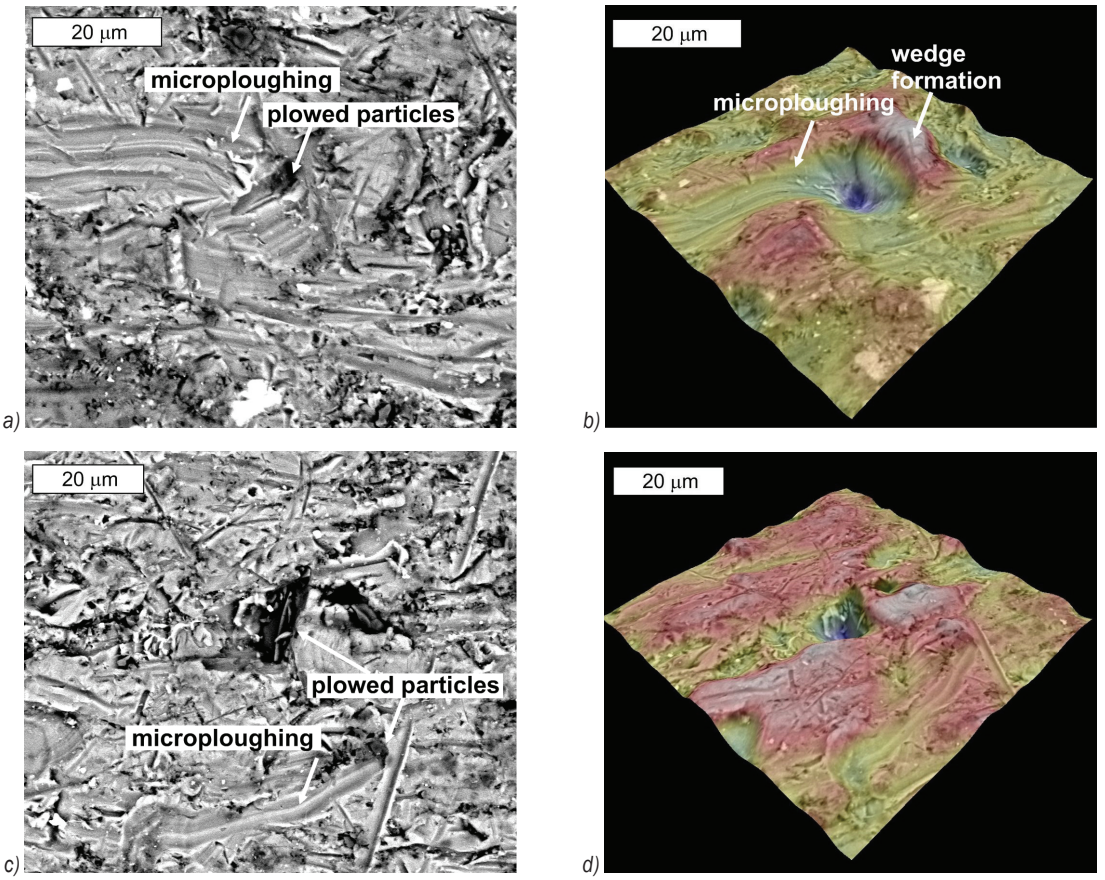

Fig. 15. *Micro-ploughing of the surface is visible in the heat treatment state; a) DA, SEM image, b) DA, SEM 3D-profilometry image, c) RRA, SEM image, and d) RRA, SEM 3D-profilometry image*

way, while moving in the mass of the material, may contribute to increased wear. Volume loss may occur as a result of the action of many abrasive particles.

2.3 Wear Surface

To understand the reason for the different wear mechanisms better and to study the influence of matrix hardness on the wear performance, the morphology of the wear track was examined using SEM analysis.

The analyses of the wear paths revealed the same type of damage in all the tested alloy states (Fig. 7), with the wear being abrasive. As shown in the images obtained at higher magnifications: grooves and scratches, microcracks, and plastic deformation can be easily observed on the surface of the wear tracks (Figs. 8 to 13). The resulting surface irregularities ranged from 4 µm to 6 µm, regardless of the heat treatment condition (Figs. 9, 11 and 13). The main wear mechanisms are therefore controlled by wedge formation and micro-ploughing (Figs. 14 and 15). However, this causes a large amount of ploughed material to embed into the matrix at the edge of the wear mark, which makes a significant contribution to material fatigue. Moreover, the abrasive material cuts the surface of the matrix. The grooves and scratches that are formed are not always parallel to the direction of friction, which indicates the displacement of the friction particles in the wear area (Fig. 7). The precipitations can increase hardness, but at the same time enhance the wear rate by causing disruption of plastic flow during particle impact. The larger ones can also act as an abrasive and, in turn, increase the wear rate during abrasion.

2.4 Subsurface Wear Morphology of the Samples and Microhardness Measurements

Observations of the wear surface carried out on the cross-section confirm the presented thesis (Figs. 16 to 20). In the case of the DA state, more even wear was observed but, at the same time, it was often accompanied by delamination, which in turn contributed to the removal of larger fragments of the wear material (Figs. 18 and 19). It is unlikely that the fragments observed in the microscopic image came from surface micro-cutting, as this mechanism was not observed on the surface in the SEM investigations. This undoubtedly contributed to the greater wear observed during the tribological tests.

As indicated earlier, the key factor was the microstructure. Observations on the perpendicular cross-section of the samples showed that decohesion developed mainly in the area of the grain boundaries and interfacial boundaries (Figs. 16b, 18b and 20c). The loss of continuity with the matrix is much easier in the case of non-coherent particles than in the presence of coherent precipitations. The tendency for intergranular crack growth is an effect of planar slip band development results from the repeated shearing of precipitates by dislocation motion [28].

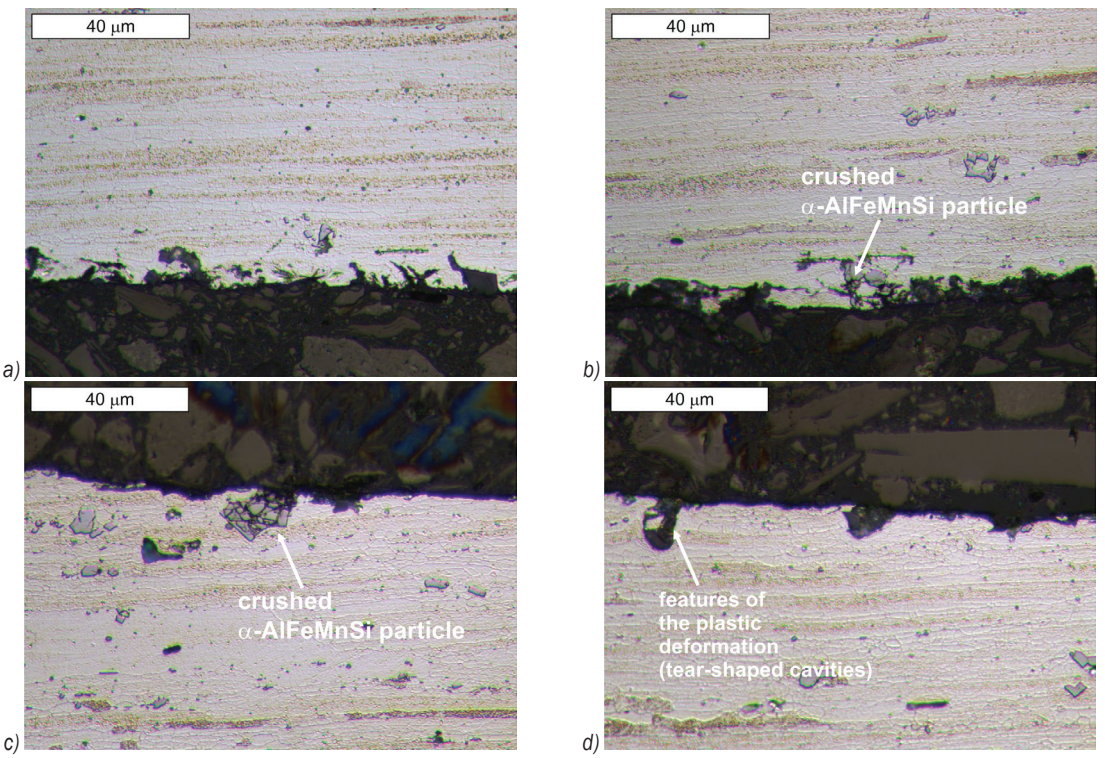

Fig. 16. *Subsurface wear morphology of the samples in the T6 state; a) and b) perpendicular, and c) and d) and parallel to the sliding direction; Light microscopy, etched with 10 % HF*

In the T6 state, which is formed mainly by coherent precipitations [4] and [29], changes typical for surface scratching and micro-ploughing were observed (Figs. 16 and 17). Although changes in the direction of the features that formed on the surface of the samples were observed, the greatest changes in the cross-section occurred in the direction perpendicular to the sliding (Figs. 16a and b). The nature of the subsurface wear morphology observed in the RRA state was similar to those in the T6 state (Fig. 20). Regardless of the heat treatment states, microstructure evolution caused by plastic deformation was not observed. Small effects of plastic deformation were observed in the places where the abrasive was pressed into the surface of the samples, which led to the formation of characteristic tear-shaped cavities (Figs. 16d and 19b). In all the samples, it was also observed that the presence of the α-AlFeMnSi particles in the subsurface area leads to

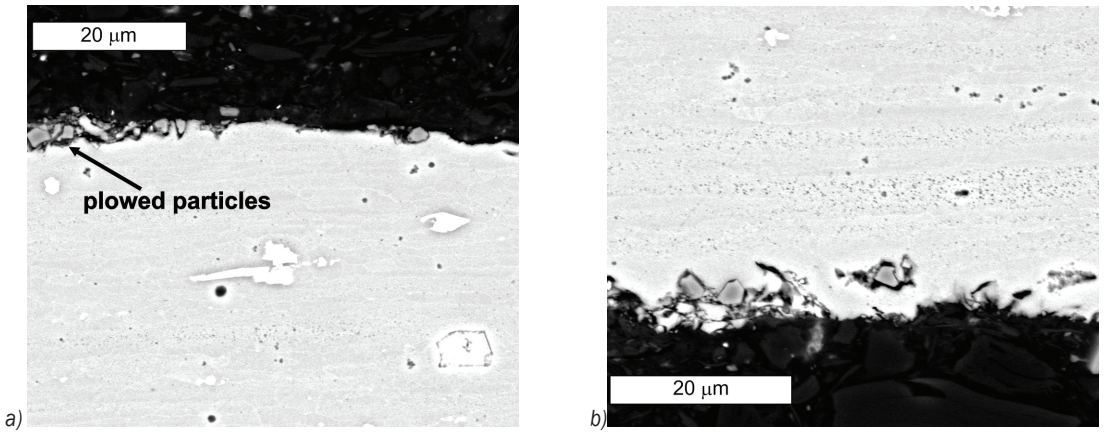

Fig. 17. *Subsurface wear morphology of the samples in the T6 state; a) parallel to the sliding direction, and b) perpendicular to the sliding direction, SEM, etched with 10 % HF*

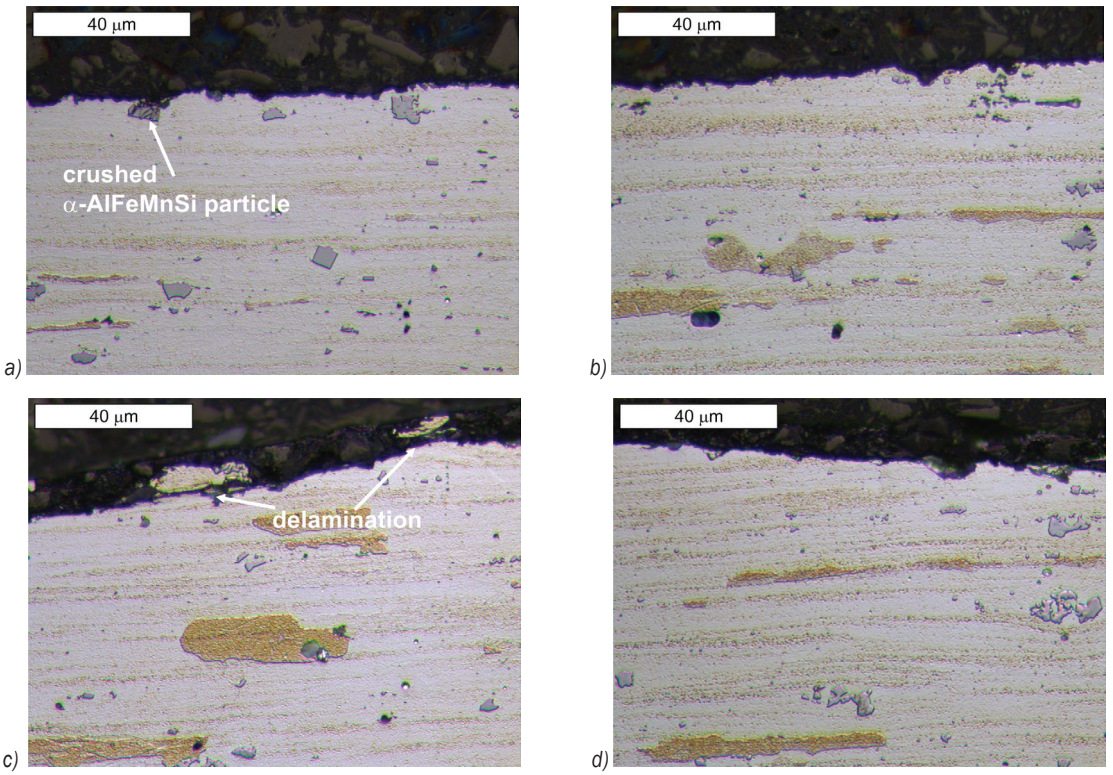

Fig. 18. *Subsurface wear morphology of the samples after double-stage aging (DA state); a) and b) perpendicular, and c) and d) parallel to the sliding direction; Light microscopy, etched with 10 % HF*

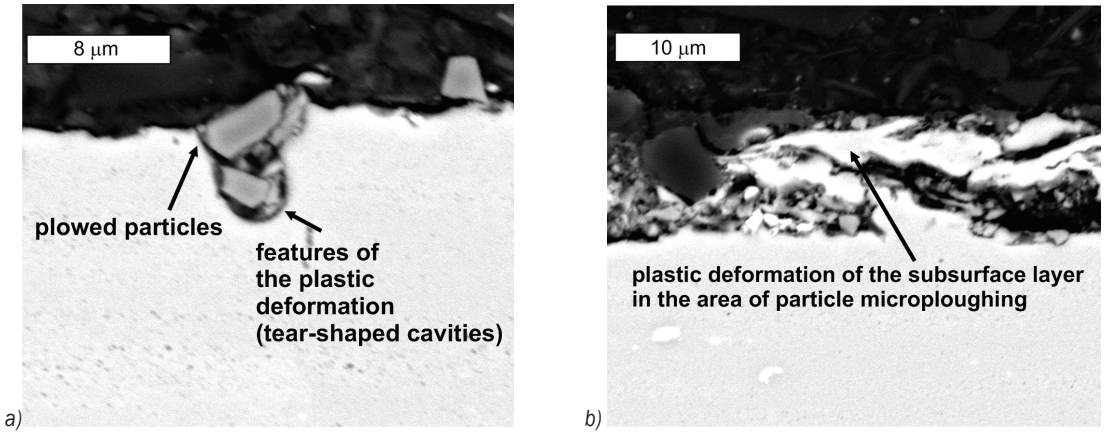

Fig. 19. *Subsurface wear morphology of the samples in the DA state; parallel to the sliding direction, SEM, etched with 10 % HF*

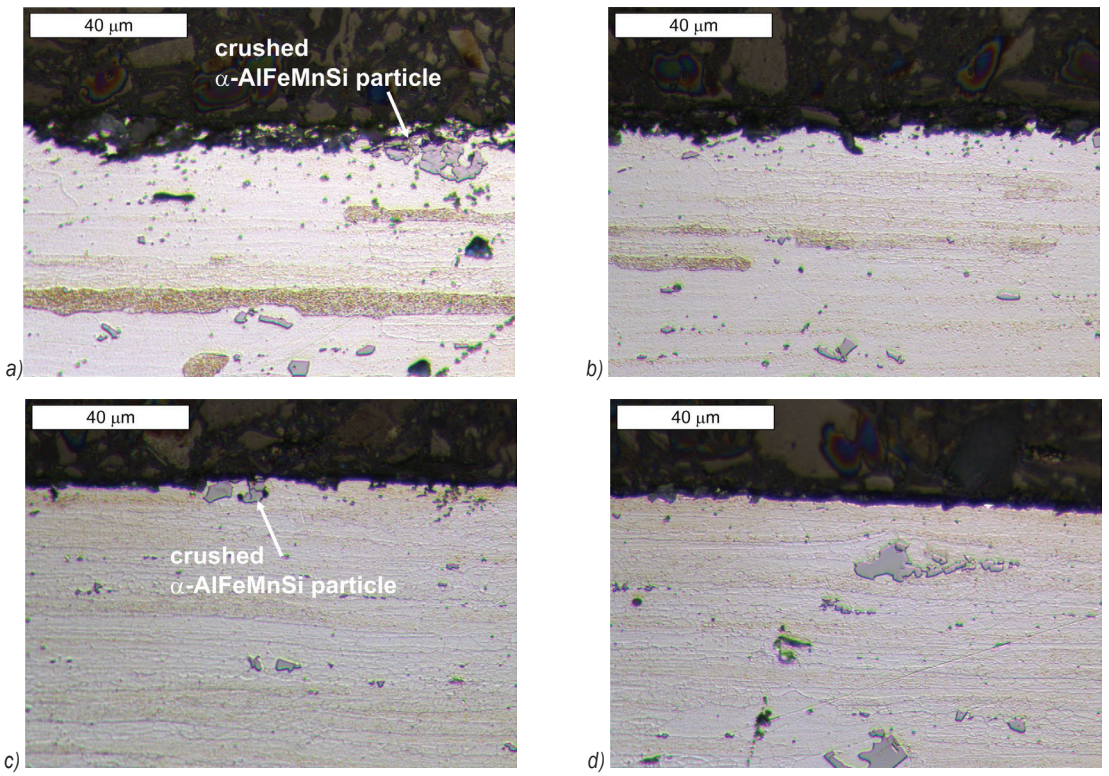

Fig. 20. *Subsurface wear morphology of the samples after RRA treatment (RRA state); a) and b) perpendicular, and c) and d) parallel to the sliding direction; light microscopy, etched with 10 % HF*

its defragmentation and crushing. This also promotes its penetration into the friction area (Figs. 16b and c, 17, 18a, and 20).

The microhardness measurements are consistent with the macrohardness measurements. The microhardness can be ranked in the following increasing order: DA <T6 <RRA. Two effects can be expected as a result of the friction: an increase in hardness in the near-surface area, which would indicate the occurrence of hardening caused by plastic deformation; and the fact that increasing the temperature during friction may result in a partial disappearance and growth of the precipitation strengthening phases. The performed studies indicate that none of these effects occurred. The hardness fluctuated due to the microstructural heterogeneity. However, no tendency to increase or decrease the hardness directly at the surface was observed. The results are shown in Fig. 21. The dashed lines are

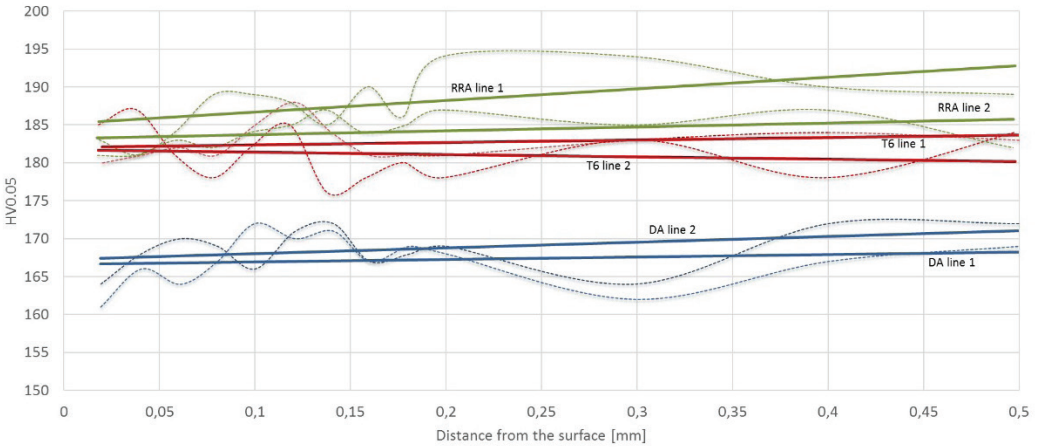

Fig. 21. *Hardness distribution curves as a function of distance from the surface*

responsible for the actual hardness distributions, while the solid line is an approximation.

3 CONCLUSIONS

The results of the hardness measurement and microscopic examinations, and the underlying reasons for the observed behaviour, can be summarized as follows:

1. The hardness of the AW7075 alloy is not the only determinant of abrasive wear. The conducted research shows that the microstructure of the tested alloy and the related heat treatment state also play an important role in this respect. The factor that favours the high value of the K_b coefficient is its high hardness, which is caused by the presence of phases that are coherent with the matrix. This parameter increases in the following order: DA <RRA <T6.
2. The analyses of the wear paths showed the same type of damage in all the tested alloy states. The scratches, grooves, microcracks, and slight features of plastic deformation can be observed on the wear surface. The main wear mechanisms are therefore controlled by wedge formation and micro-ploughing. The delamination tendency may also have contributed to the increased wear of the DA condition, as delamination was observed in this condition. This is most likely related to the fact that this state has the lowest hardness.
3. The incoherent precipitation can increase hardness, as well as the wear rate, by disturbing the plastic flow during particle impact. Larger particles can also act as an abrasive and increase the wear rate during abrasion. Observations on the perpendicular cross-section of the samples showed that decohesion developed mainly around the grain boundaries and interfacial boundaries. The loss of continuity with the matrix is much easier in their case than in the presence of coherent particles.
4. The presence of large precipitates of the primary phases, which do not dissolve at the stage of heat treatment, favours their crushing and defragmentation during abrasive wear. This promotes their penetration into the friction area.
5. No tendency of an increase or decrease of the hardness directly at the surface was observed. An increase in hardness in the near-surface area could be expected, which would indicate the occurrence of hardening due to plastic deformation. However, an increase in temperature during wear could cause a partial disappearance and growth of the precipitation strengthening phases, which would result in a decrease in surface hardness. The studies performed indicate that none of these effects occurred.

4 REFERENCES

[1] Leśniewski, T. (2013). The influence of hardness of the steel sliding surfaces on their tribological characteristics. *5th World Tribology Congress*, p. 1-4.

[2] Lachowicz, M.M., Leśniewski, T., Lachowicz, M.B., Jasionowski, R. (2020). Tribological wear of as cast Zn-4Al alloy cooled at various rates from the eutectoid transformation temperature. *Archives of Foundry Engineering*, vol. 20, no. 4, p. 108-114, **DOI:10.24425/afe.2020.133356**.

[3] Krawczyk, J. (2010). Influence of the microstructure and loads on tribological properties of G155CrNiMo4-3-3 cast steel. *Archives of Foundry Engineering*, vol. 10, no. 3, p. 39-44.

[4] Yang, W., Ji, S., Wang, M., Li, Z. (2014). Precipitation behaviour of Al-Zn-Mg-Cu alloy and diffraction analysis from η′

precipitates in four variants. *Journal of Alloys and Compounds*, vol. 610, p. 623-629, **DOI:10.1016/j.jallcom.2014.05.061**.

[5] Berg, L.K., Gjønnes, J, Hansen, V, Li, X.Z, Knutson-Wedel, M., Waterloo, G., Schryvers, D., Wallenberg, L.R. (2001). GP-zones in Al-Zn-Mg alloys and their role in artificial aging. *Acta Materialia*, vol. 49, no 17, p. 3443-3451, **DOI:10.1016/S1359-6454(01)00251-8**.

[6] Peng, G., Chen, K., Chen, S., Fang, H. (2011). Influence of repetitious-RRA treatment on the strength and SCC resistance of Al-Zn-Mg-Cu alloy. *Materials Science and Engineering: A*, vol. 528, no. 12, 2011, p. 4014-4018, **DOI:10.1016/j.msea.2011.01.088**.

[7] Guo, F., Duan, S., Wu, D., Matsuda, K., Wang, T., Zou, Y. (2020). Effect of retrogression re-aging treatment on corrosion behavior of 7055 Al-Zn-Mg alloy. *Materials Research Express*, vol. 7, no 10, art. ID 106523, **DOI:10.1088/2053-1591/abc191**.

[8] Ashby, M.F., Jones, D.R.H. (2013). *Engineering Materials 2 - An Introduction to Microstructure and Processing*. Elsevier, Oxford.

[9] Ozer, G., Karaaslan, A. (2017). Properties of AA7075 aluminum alloy in aging and retrogression and reaging process. *Transactions of Nonferrous Metals Society of China*, vol. 27, no. 11, p. 2357-2362, **DOI:10.1016/S1003-6326(17)60261-9**.

[10] Park, J.K., Ardell, A.J. (1984). Effect of retrogression and reaging treatments on the microstructure of Ai-7075-T651. *Metallurgical and Materials Transactions A*, vol. 15, p. 1531-1543, **DOI:10.1007/BF02657792**.

[11] Marlaud, T., Deschamps, A., Bley, F., Lefebvre, W., Baroux, B. (2010). Evolution of precipitate microstructures during the retrogression and re-ageing heat treatment of an Al-Zn-Mg-Cu alloy. *Acta Materialia*, vol. 58, no. 14, p. 4814-4826, **DOI:10.1016/j.actamat.2010.05.017**.

[12] Wang, Y.L., Jiang, H.C., Li, Z.M., Yan, D.S., Zhang, D., Rong, L.J. (2018). Two-stage double peaks ageing and its effect on stress corrosion cracking susceptibility of Al-Zn-Mg alloy. *Journal of Materials Science & Technology*, vol. 34, no. 7, p. 1250-1257, **DOI:10.1016/j.jmst.2017.05.008**.

[13] Emani, S.V., Benedyk, J., Nash, P., Chen, D. (2009). Double aging and thermomechanical heat treatment of AA7075 aluminum alloy extrusions. *Journal of Materials Science*, vol. 44, p. 6384-6391, **DOI:10.1007/s10853-009-3879-8**.

[14] Umamaheshwer Rao, A.C., Vasu, V., Govindaraju, M., Sai Srinadh, K.V. (2016). Stress corrosion cracking behaviour of 7xxx aluminum alloys: A literature review. *Transactions of Nonferrous Metals Society of China*, vol. 26, no. 6, p. 1447-1471, **DOI:10.1016/S1003-6326(16)64220-6**.

[15] Krishnanunni, S., Gupta, R.K., Ajithkumar, G., Anil Kumar, V., Ghosh, R. (2020). Investigation on effect of optimized RRA in strength and SCC resistance for aluminium alloy AA7010. *Materials Today: Proceedings*, vol. 27, p. 2385-2389, **DOI:10.1016/j.matpr.2019.09.136**.

[16] Ładak, A., Cichoń, M., Lachowicz, M.M. (2022). Evaluation of the effect of dual-stage aging and RRA on the hardening and corrosion resistance of AW7075 Alloy. *Corrosion and Materials Degradation*, vol. 3, no. 1, p. 142-159, **DOI:10.3390/cmd3010008**.

[17] Li, Y., Xu, G., Liu, S., Peng, X., Yin, Z., Wang, L., Liang, X. (2019). Effect of ageing treatment on fatigue crack growth of die forged Al-5.87Zn-2.07Mg-2.42Cu alloy. *Engineering Fracture Mechanics*, vol. 215, p. 251-260, **DOI:10.1016/j.engfracmech.2019.04.023**.

[18] Nandana, M.S., Udaya Bhat, K., Manjunatha, C.M. (2019). Influence of retrogression and re-ageing heat treatment on the fatigue crack growth behavior of 7010 aluminum alloy. *Procedia Structural Integrity*, vol. 14, p. 314-321, **DOI:10.1016/j.prostr.2019.05.039**.

[19] Wang, Y., Liu, M., Xiao, W., Zhao, W., Ma, C. (2020). Effects of multi-stage aging treatments on the precipitation behavior and properties of 7136 aluminum alloy. *Journal of Alloys and Compounds*, vol. 814, art. ID 152256, **DOI:10.1016/j.jallcom.2019.152256**.

[20] Li, Z., Yu, H., Sun, D. (2021). The tribocorrosion mechanism of aluminum alloy 7075-T6 in the deep ocean. *Corrosion Science*, vol. 183, art. ID 109306, **DOI:10.1016/j.corsci.2021.109306**.

[21] GOST 23.208-79: Ensuring of wear resistance of products. Wear resistance testing of materials by friction against loosely fixed abrasive particles. Euro-Asian Council for Standardization, Metrology and Certification.

[22] Gore, G.J., Gates, J.D. (1997). Effect of hardness on three very different forms of wear. *Wear*, vol. 203-204, p. 544-563, **DOI:10.1016/S0043-1648(96)07414-5**.

[23] Mezlini, S., Kapsa, Ph., Henon, C., Guillemenet, J. (2004). Abrasion of aluminium alloy: effect of subsurface hardness and scratch interaction simulation. *Wear*, vol. 257, no. 9-10, p. 892-900, **DOI:10.1016/j.wear.2004.05.004**.

[24] Elleuch, K., Mezlini, S., Guermazi, N., Kapsa, Ph. (2006). Abrasive wear of aluminium alloys rubbed against sand. *Wear*, vol. 261, no. 11-12, p. 1316-1321, **DOI:10.1016/j.wear.2006.03.016**.

[25] Suleiman, I.Y., Kasim, A., Mohammed, A.T., Sirajo, M.Z. (2021). Evaluation of mechanical, microstructures and wear behaviours of aluminium alloy reinforced with mussel shell powder for automobile applications. *Strojniški vestnik - Journal of Mechanical Engineering*, vol. 67, no. 1-2, p. 27-35, **DOI:10.5545/sv-jme.2020.6953**.

[26] Udoye, N.E. Fayomi, O.S.I., Inegbenebor, A.O. (2019). Assessment of wear resistance of aluminium alloy in manufacturing industry - A review. *Procedia Manufacturing*, vol. 35, p. 1383-1386, **DOI:10.1016/j.promfg.2019.09.00721**.

[27] Chotěborský, R., Hrabě, P., Müller, M., Savková, J., Jirka, M., Navrátilová, M. (2009): Effect of abrasive particle size on abrasive wear of hardfacing alloys. *Research in Agricultural Engineering*, vol. 55, p. 101-113, **DOI:10.17221/24/2008-RAE**.

[28] Ku, A.Y., Khan, A.S., Gnäupel-Herold, T. (2020). Quasi-static and dynamic response, and texture evolution of two overaged Al 7056 alloy plates in T761 and T721 tempers: Experiments and modeling. *International Journal of Plasticity*, vol. 130, art. ID 102679, **DOI:10.1016/j.ijplas.2020.102679**.

[29] Chen, J., Zhen, L., Yang, S., Shao, W., Dai, S. (2009). Investigation of precipitation behavior and related hardening in AA 7055 aluminum alloy. *Materials Science and Engineering: A*, vol. 500, no. 1-2, p. 34-42, **DOI:10.1016/j.msea.2008.09.065**.